Journal of Inflammation Research

Dovepress
Taylor & Francis Group

Open Access Full Text Article

ORIGINAL RESEARCH

Mechanistic Study of CD90-Positive Synovial Fibroblasts in the Invasion and Recurrence of Pigmented Villonodular Synovitis

Lingkai Kong[1,*], Hantao Chen[1,*], Hengbo Zhang[2,*], Xi Zhang[3], Junhao Chen[1], Yi Nie[1], Zexin Su[1], Lijun Lin[1]

[1]Department of Joint and Orthopedics, Zhujiang Hospital, Southern Medical University, Guangzhou, 510282, People's Republic of China; [2]Department of Orthopedic and Traumatology, Zhujiang Hospital, Southern Medical University, Guangzhou, 510282, People's Republic of China; [3]Department of Pediatric Surgery, Zhujiang Hospital, Southern Medical University, Guangzhou, Guangdong, 510282, People's Republic of China

*These authors contributed equally to this work

Correspondence: Zexin Su; Lijun Lin, Department of Joint and Orthopedics, Zhujiang Hospital, Southern Medical University, Guangzhou, 510282, People's Republic of China, Email szx2343661@163.com; Gost1@smu.edu.cn

Objective: Pigmented villonodular synovitis (PVNS), also known as tenosynovial giant cell tumor (TGCT), is a rare, locally aggressive mesenchymal tumor. The pathogenesis of PVNS remains poorly understood, significantly limiting current therapeutic options.

Methods: In the present study, gene expression profiles of PVNS and Osteoarthritis (OA) synovium from GSE3698, GSE175626 and GSE176133 were analyzed using integrating RNA sequencing (RNA-seq) and microarray to investigate the PVNS transcriptome. Differentially expressed genes (DEGs) were identified, gene set enrichment analysis (GSEA) and KEGG pathway enrichment analysis were used to determine the gene functional enrichment. CIBERSORT algorithm was executed to evaluate the characteristics of tissue immune infiltration. Immunohistochemical staining was used to evaluate inflammatory cell infiltration and immunofluorescence staining was used to identify the synovial fibroblasts (FLSs) derived from PVNS synovium. Additionally, Western blot, flow cytometry, immunofluorescence analysis, transwell migration and invasion assays, and wound-healing assays were performed to further explore the difference of CD90+PDPN+ FLSs between OA and PVNS.

Results: According to GSEA analysis and pathway enrichment analysis, the most significant manifestations of PVNS synovium were inflammatory infiltration and bone resorption. Increased immune cells infiltration including M2 macrophages and Neutrophils were observed through CIBERSORT algorithm and validated through immunohistochemical staining. Subsequently, scRNA-seq data was analyzed to identify 16 cell subpopulations and reveal increased proportion of CD90+PDPN+ FLS in PVNS synovium. CD90+PDPN+ FLSs in PVNS can secrete inflammatory factors, degrade bone, and exhibit invasive characteristics. These cells, typically located in the sublining layer, highly expressed IL-1β, TNF-α, M-CSF and MMP9, while expressing less OPG.

Conclusion: This study elucidates the structure of the PVNS synovium compared to OA synovium and highlights the crucial role of CD90+PDPN+ FLSs in synovial invasion and bone resorption. These findings may lead to updated treatment concepts for PVNS and reveal new therapeutic targets. This study opens promising avenues for developing targeted therapeutic strategies aimed at inhibiting the invasive and osteoclastogenic functions of CD90+PDPN+ FLSs in PVNS. Future research should focus on validating these cells as potential therapeutic targets, possibly through the use of selective inhibitors, which could help mitigate synovial hyperplasia and bone destruction in affected patients.

Keywords: pigmented villonodular synovitis, CD90, PDPN, synovial fibroblasts, synovial invasion, bone resorption

Introduction

Pigmented villonodular synovitis (PVNS) is a rare, locally aggressive synovial tumor that primarily affects the synovium, bursa, or tendon sheath of joints.[1] The annual incidence of PVNS is estimated to be 18 cases per million population, with

Received: 27 June 2025
Accepted: 2 December 2025
Published: 8 December 2025

approximately 70% being of the diffuse subtype.[2] It is most commonly found in the knee joint but can also occur in the hip, elbow, and ankle joints.[3] A subset of cells in PVNS exhibit neoplastic characteristics and aberrantly express colony-stimulating factor 1 (CSF1) due to genomic alterations at the CSF1 locus on chromosome 1p13.[4] This dysregulated CSF1 attracts histiocyte-like cells and inflammatory cells, which constitute majority of the tumor mass and may ultimately lead to joint effusion, swelling, and pain.[5] However, current treatments for PVNS, which primarily involve open or arthroscopic synovectomy, are associated with high recurrence rates. This underscores the need for more targeted therapeutic strategies to improve long-term outcomes.[2]

Due to the low incidence and atypical clinical features of PVNS, the current understanding of its pathogenesis remains unclear.[6] A previous analysis using genome-wide complementary DNA microarray and tissue array found that the gene expression profiles of PVNS synovium were significantly different from those of Rheumatoid arthritis (RA) and Osteoarthritis (OA) tissues, and pointed out that the gene expression signature in PVNS is similar to activated macrophages, consistent with the pathological features of the disease.[7] Integrated transcriptome bioinformatics analysis conducted by Zhao et al showed that the transcriptional expression characteristics of PVNS are manifested as enhanced immune response, cell migration, and osteoclastogenesis, and the expression of MMP9, SIGLEC 15, and RANK in PVNS myeloid cells is higher than that in OA.[8] Through machine learning and bioinformatics analysis, Heng et al found that PLIN, PPAP2A, and TYROBP may affect RA and PVNS by regulating immunity, and contribute to the diagnosis and treatment of these two diseases.[9] However, the detailed molecular mechanism of PVNS has not been elucidated, and its essential differences from other inflammatory diseases such as RA and OA have not been studied in detail.[6] Therefore, it is necessary to elucidate the pathological mechanism of PVNS and provide useful insights for its diagnosis and treatment.

In this study, we found significant overexpression of inflammatory response and bone destruction related pathways in the synovium of PVNS patients by integrating transcriptome bioinformatics analysis. Additionally, we observed a substantial accumulation of neutrophils and M2 macrophages within the synovium of PVNS. Our results also showed that CD90+PDPN+ FLSs is highly expressed in PVNS patients and is positively correlated with increased invasiveness, inflammation mediation, and bone destruction. These findings demonstrated that CD90+PDPN+ FLSs is a key factor in the regulation of PVNS inflammation and is involved in PVNS pathogenesis, potentially providing a promising prognostic and therapeutic strategy for PVNS treatment.

Materials and Methods

Collection of Gene Expression Datasets

Clinical data and gene expression matrices of PVNS and OA patients were downloaded from Gene Expression Omnibus (GEO, https://www.ncbi.nlm.nih.gov/geo/) databases. After dataset screening, three public datasets were used for integrated bioinformatics analysis in this study, including GSE3698, GSE175626, and GSE176133. GSE3698 contains a total of 48 synovium, including 19 OA patients, 18 RA patients and 11 PVNS patients. GSE175626 contains 3 synovium from OA patients and 3 synovium from PVNS patients. GSE176133 contains 3 synovium from OA patients and 3 synovium from PVNS patients. On the other hand, the scRNA-seq dataset GSE155527 was also download from GEO database which contains 3 synovium from OA patients and 5 synovium from PVNS patients.

Gene Set Enrichment Analysis (GSEA)

The patients were split into PVNS and OA groups according to different sources of disease. GSEA (software.broadinstitute.org/gsea/index.jsp) was used to determine whether the pre-defined HALLMARK and Gene ontology pathways were enriched. The enrichment scores, normalized enrichment scores and P-values were calculated. $P<0.05$ and a false discovery rate $q<0.05$ were considered to indicate a statistically significant difference.

Identification of Differentially Expressed Genes (DEGs)

The limma package version 3.42.0 (bioconductor.org/packages/release/bioc/html/limma.html) was used to identify differentially expressed genes between PVNS and OA groups using the following cutoffs: $|\log_2$ fold change (FC)$|\geq 1$

and P<0.05. The intersection genes that were differentially expressed (up- or downregulated) between the groups were identified using the VennDiagram package version 1.6.20 (https://CRAN.R-project.org/package=VennDiagram).

Kyoto Encyclopedia of Genes and Genomes (KEGG) Enrichment Analyses

To identify the functions and pathways associated with the intersecting genes, we performed KEGG pathway enrichment analyses using the clusterProfiler package (version 3.14.2) (bioconductor.org/packages/release/bioc/html/clusterProfiler.html). Statistical significance was determined by a P-value threshold of less than 0.05.

Evaluation of Immune Infiltration

Using an online analytical platform CIBERSORT (https://cibersortx.stanford.edu/), the compositional proportion of immune infiltrating cells in the PVNS, RA and OA synovium of dataset GSE3698 were calculated based on the characteristic gene set of 22 immune cell subtypes. According to the relative abundances of 22 immune infiltrating cells, the differences in immune cell infiltration between PVNS and OA groups were analyzed. P value < 0.05 was regarded as a statistically significant difference.

Analysis of scRNA-Seq Dataset

The scRNA-seq dataset was processed in R software using the "Seurat" package. Following stringent quality control measures and data filtering, we performed principal component analysis (PCA) on the 2000 most highly variable genes to discern the most pertinent principal components (PCs). Subsequently, t-distributed stochastic neighbor embedding (t-SNE) was used for unsupervised clustering and an unbiased visualization of cell subpopulations. The differential expressed genes between clusters was analyzed using the "FindAllMarkers" function. Additionally, subpopulations within each cluster were annotated using the "SingleR" package.

Patients

In this study, we collected synovium samples from 6 patients with PVNS, 6 patients with OA, and 3 patients with anterior cruciate ligament (ACL) injuries. All samples were collected under protocols approved by the Ethics Committee of Zhujiang Hospital, affiliated with Southern Medical University, with informed consent obtained from all patients. The synovium was sourced from patients who had undergone arthroscopic synovectomy and total knee arthroplasty for further culture of FLSs, histological examination, and immunofluorescence experiments.

Cell Isolation and Culture

Synovial fibroblasts (FLSs) were isolated from the synovium of PVNS and OA patients through enzymatic digestion. Within 2 hours of arthroscopic collection, the synovium was minced into a slurry and incubated with 2 mg/mL type I collagenase (Solarbio, China, C8140) in 2 mL of high-glucose Dulbecco's modified Eagle's medium (DMEM, Gibco, China, C11995500BT) at 37°C on a shaker for 2–4 hours. To stop the digestion, 4 mL of complete medium (DMEM supplemented with 10% fetal bovine serum (FBS, Invitrogen, Australia, 10099141C), 100 U/mL penicillin, and 100 μg/mL streptomycin) was added. The mixture was centrifuged at 2500 rpm to remove the supernatant and floating adipose tissue. The pellet was then resuspended in complete medium and cultured in an incubator at 37°C with 5% CO2. Primary cell migration from the adherent explants was observed under a microscope 3 days post-seeding, with the cells reaching over 50% confluence by day 7. At 90% confluency, FLSs were isolated from primary cultures by flow cytometry sorting (Beckman, America, Z36434), achieving >95% purity. After the second passage, non-FLSs were completely eliminated, leaving primarily FLSs.

Immunohistochemical/Immunofluorescence Staining

The synovium was fixed with 4% formaldehyde overnight. After fixation, the tissues were embedded in paraffin and sectioned. The paraffin sections were baked, deparaffinized, hydrated, and treated with 0.1% trypsin (Gibco, China, 25200072) at 37°C for 30 minutes for antigen retrieval. After washing with PBS three times, 3% hydrogen peroxide was added for 15 minutes to quench endogenous peroxidase activity. The sections were blocked with Biyuntian commercial

blocking solution at room temperature for 2 hours. Primary antibodies were incubated overnight at 4°C. The primary antibodies used were: mouse anti-human CD90 (1:100; Proteintech, China, 66766-1-Ig) and rabbit anti-human PDPN (1:100; Proteintech, China, 11629-1-AP) for immunofluorescence staining; mouse anti-human CD206 (1:100; Proteintech, China, 18704-1-AP) and rabbit anti-human CXCR2 (1:100; Proteintech, China, 20634-1-AP) for immunohistochemical staining. Secondary antibodies for immunofluorescence staining were Alexa Fluor Plus 488 goat anti-rabbit IgG (1:200; Bioss, China, bs-0295G-BF488) and Alexa Fluor Plus 594 goat anti-mouse IgG (1:200; Bioss, China, bs-0296G-BF594). For immunohistochemical staining, HRP-conjugated goat anti-rabbit IgG (1:200; Fdbio Science, China, FDR007) and HRP-conjugated goat anti-mouse IgG (1:200; Fdbio Science, China, FDM007) were used. Samples were incubated at room temperature for 30 minutes (protected from light for immunofluorescence staining). The samples were then stained with DAB (OriGene, America, ZLI-9018) or DAPI (Solarbio, China, S2110). Signals were visualized and images acquired using a Leica microscope. Primary cells were cultured on coverslips in 6-well plates. At over 80% confluence, cells were fixed for 30 minutes, permeabilized with 0.1% Triton X-100 (Biofroxx, Germany, 1139ML100) for 1 hour, and incubated with primary antibodies at 4°C overnight. After incubation with fluorescent secondary antibodies for 1 hour, the coverslips were mounted with DAPI-containing anti-fade medium and imaged under a Nikon confocal microscope. All experiments were independently repeated three times. Each replicate utilized matched samples from individual patients: one PVNS and one OA sample for the IHC and cell climb IF assays, with the tissue IF assay additionally including one anterior cruciate ligament (ACL) injury sample as a normal control in each replicate.

Flow Cytometry and Cell Sorting

Primary cells cultured in 75 cm^2 flasks were washed twice with PBS and digested with trypsin. Digestion was stopped with complete medium, and cells were counted to 1 million cells. Cells were centrifuged (300g for 5 minutes) to remove the supernatant and resuspended in 200 μL of 4% formaldehyde (approximately 100 μL for every 1 million cells). Cells were transferred to a 1.5 mL EP tube and mixed on a shaker. Fixation was done at room temperature for 15 minutes. After centrifugation to remove formaldehyde, cells were washed twice with staining buffer (0.5 g BSA (MRC, China, CCS30014.01D) + 50 mL PBS). Cells were permeabilized with permeabilization solution (1 μL Triton X-100 in 1 mL staining buffer) while adding flow cytometry-specific primary antibodies (5 μL each of anti-CD90 (BioLegend, China, 328107) and anti-PDPN (BioLegend, China, 337021)) and incubated at room temperature for 30 minutes in the dark. Cells were washed twice with staining buffer and resuspended in 500 μL staining buffer for flow cytometry analysis. Samples were filtered through a 70 μm cell strainer before analysis. Based on the flow cytometry analysis results, the primary cell pellet obtained after trypsin digestion was resuspended in PBS. Primary antibodies were added at a ratio of 5 μL per 1 million cells, followed by thorough mixing and incubation at room temperature for 30 minutes in the dark. After two washes with PBS, the cell suspension was transferred to a flow sorting tube. High-purity FLSs were then isolated using a cell sorter for subsequent experiments. Independent experiments were performed in triplicate. For each experiment, primary cells from one PVNS patient and one OA patient were analyzed. In total, cells from three PVNS and three OA patients were used.

Migration and Invasion Assays

The migration and invasion abilities of PVNS and OA FLSs were determined using Transwell plates with 10-mm diameter and 8.0-μm pore polycarbonate filter inserts (FALCON, America, REF353097). For the invasion assay, the filter membrane in the upper compartment of each Transwell was coated with 25 μg of Matrigel (dilution ratio 40:1; Biosharp, China, BL1834B) and incubated at 37°C to form a reconstituted basement membrane. Cells (4×10^4 cells in 100 μL DMEM) were seeded into the upper compartments with 500 μL serum-free DMEM, while the lower compartments were filled with 600 μL DMEM supplemented with 10% FBS. After 12 hours of incubation, cells were fixed with 4% paraformaldehyde for 30 minutes and stained with 0.1% crystal violet for 20 minutes. Non-migrated cells were carefully removed from the upper surface of the Transwell filter membrane with a wet cotton swab. Cells that penetrated to the lower surface of the filter membrane were counted under a high-power (20×) microscope in six fields per well. For the migration assay, cells (2×10^4 cells in 100 μL DMEM) were seeded into the upper compartments with 500 μL serum-free DMEM, while the lower compartments were filled with 800 μL DMEM supplemented with 10% FBS. After 12 hours of

incubation, the same fixation and staining procedures were followed. The experiment was repeated three times independently, with each replicate utilizing FLSs from two different PVNS and two different OA patients (totaling six patients per group).

Wound-Healing Assay

PVNS and OA FLSs were seeded into 6-well plates. After the cells reached full confluence, a straight wound was created in each well using a 1 mL sterile pipette tip. The wounded areas were imaged under a microscope at 0, 12, and 24 hours post-scratching to assess cell migration. Independent experiments were performed in triplicate. For each experiment, FLSs from one PVNS patient and one OA patient were analyzed.

Western Blot Analysis

Second-generation PVNS and OA cells (2×10^6 cells per well) were plated into six-well plates and incubated at 37°C in 5% CO2 for 24 hours. Each well received 40 μL cell lysis buffer (RIPA lysis buffer: protease inhibitor mixture: PMSF = 100:1:1 (Fdbio Science, China, FD008; FD1001; FD0100)) and was lysed at 4°C for 30 minutes. Total cell lysates were collected, and protein concentrations were determined using a BCA protein assay kit (Abbkine, China, KTD3010). The antibodies used were as follows: rabbit anti-human PDPN (1:2000; Proteintech, China, 11629-1-AP), mouse anti-human CD90 (1:1000; Proteintech, China, 66766-1-Ig), rabbit anti-human GAPDH (1:10,000; Proteintech, China, 81640-5-RR), rabbit anti-human M-CSF (1:1000; Abcam, China, ab233387), rabbit anti-human OPG (1:1000; Affinity, China, DF6824), rabbit anti-human MMP9 (1:3000; Proteintech, China, 10375-2-AP), mouse anti-human TNF-α (1:4000; Proteintech, China, 60291-1-Ig), and rabbit anti-human IL-1β (1:2000; Proteintech, China, 26048-1-AP). Independent experiments were performed in triplicate. For each experiment, FLSs from two PVNS patients and two OA patients were analyzed. In total, FLSs from six PVNS and six OA patients were used.

Statistical Analysis

Statistical analysis was performed using GraphPad Prism (version 10.1.2) and SPSS (version 22.0). Intergroup comparisons were analyzed by unpaired Student's *t*-test. All data are expressed as mean ± standard deviation.

Results

The Inflammatory and Bone Destruction-Related Pathways of PVNS are Significantly Upregulated

To detect the distinct biological processes and signaling pathways between PVNS and OA synovium, we conducted GSEA analysis on three different datasets (GSE3698, GSE175626 and GSE176133). In the GSEA analysis of biological processes, PVNS synovium showed higher immune cell activation and bone destruction related functions (Figure 1A). In the results related to molecular signaling pathways, PVNS showed higher expression of inflammation related pathways (Figure 1B). Subsequently, differential gene analysis showed that there were 38 common differentially expressed genes between PVNS and OA synovium (Figure 1C). KEGG pathway enrichment analysis result also suggests that these differentially expressed genes are related to inflammatory response and bone destruction (Figure 1D).

Higher Inflammatory Cell Infiltration in PVNS Synovium Compared to OA Synovium

The proportions of different immune cells types were calculated by CIBERSORT in dataset GSE 3698 (Figure 2A). After organizing the immune infiltration patterns, PVNS synovium and OA synovium showed significantly different immune cell infiltration profiles (Figure 2B). Among them, PVNS synovium showed higher infiltration of M2 macrophages and neutrophils. To further validate this analysis, we performed immunohistochemical staining and the results indicated that the expression levels of CD206 and CXCR2 in PVNS synovium were significantly higher than in OA synovium (Figure 2C and D). This suggests that the infiltration of M2 macrophages and neutrophils in PVNS tissue is much higher than in OA synovium.

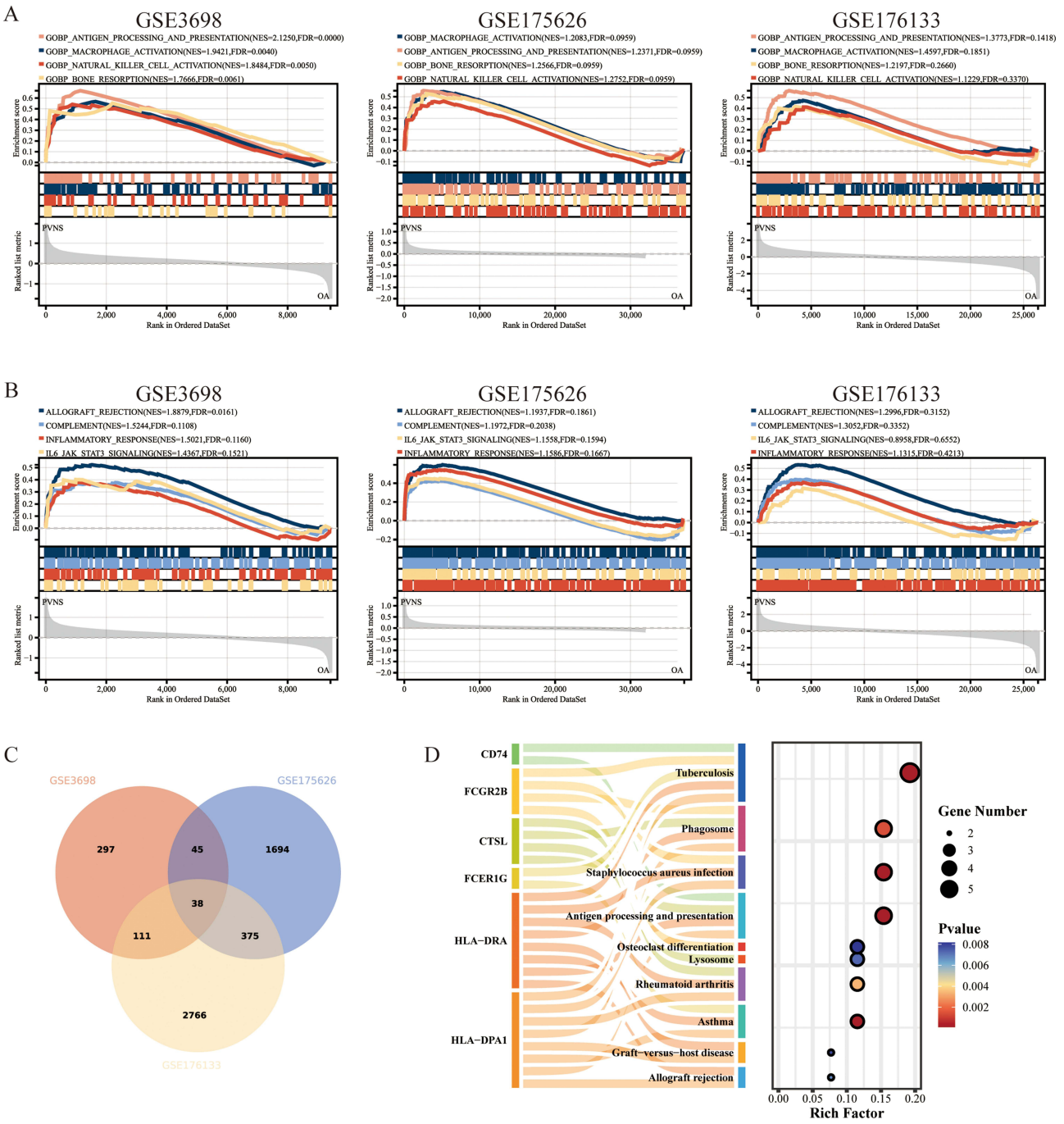

Figure 1 The inflammatory and bone destruction-related pathways are significantly upregulated in PVNS patients. (**A**) GSEA plots depicting the enrichment of upregulated biological processes of each dataset in PVNS patients. (**B**) GSEA plots depicting the enrichment of upregulated Hallmark molecular pathways of each dataset in PVNS patients. (**C**) Venn diagram of DEGs between PVNS synovium and OA synovium in GSE3698, GSE175626 and GSE176133. (**D**) KEGG pathway analysis of the common DEGs.

A High Abundance of PDPN+CD90+ FLSs in PVNS Synovium is Revealed Based on scRNA-Seq Data

We next used scRNA-seq data to identify the underlying modulators in the PVNS synovium that contribute to inflammatory response and bone destruction. After quality control and processing to eliminate batch effects (Figure 3A), we clustered cells into 16 main clusters based on the reported cell markers (Figure 3B–D). Our single-cell transcriptomic analysis found that the proportion of sublining FLS in PVNS synovium was significantly higher than

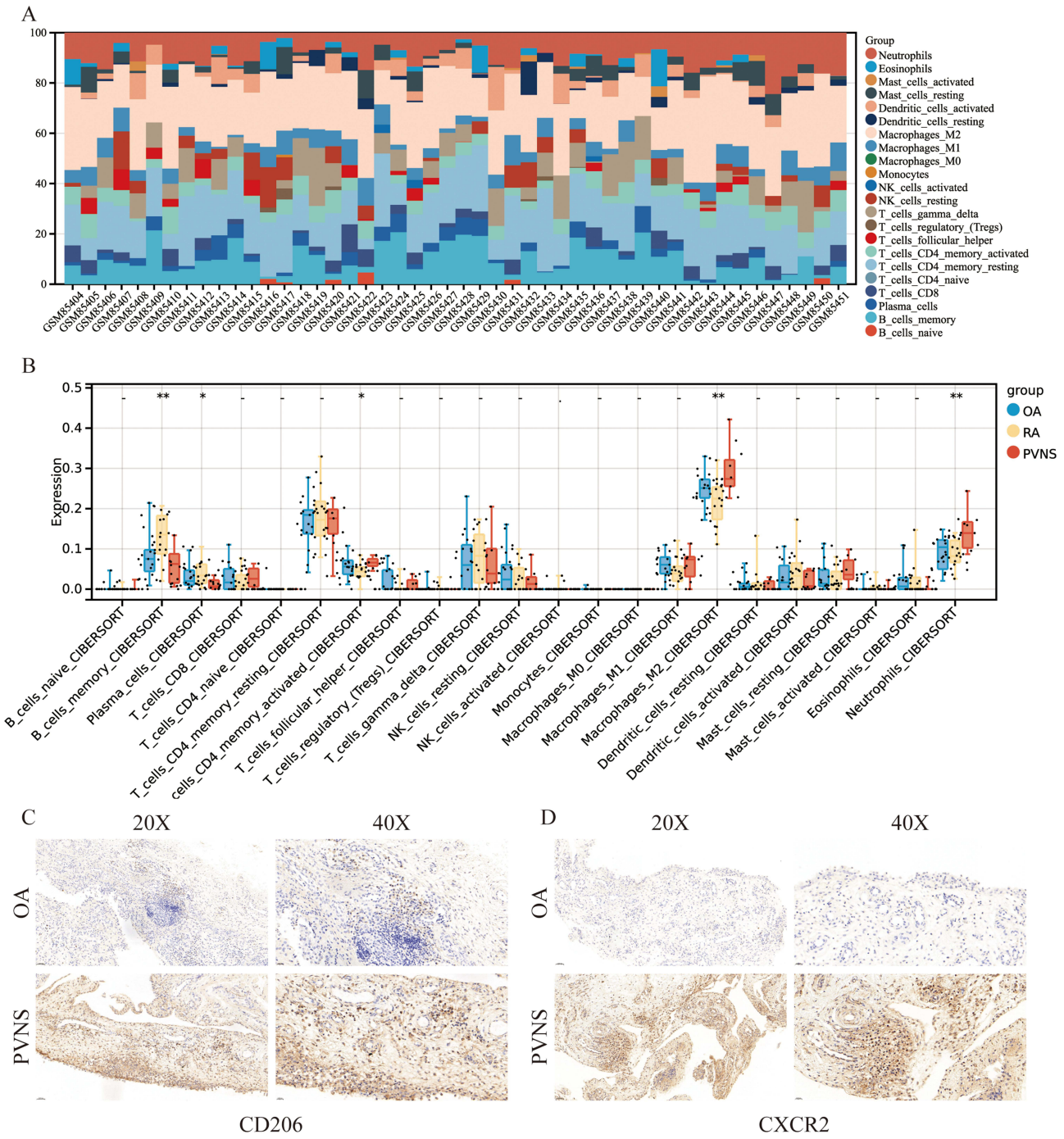

Figure 2 Inflammatory cell infiltration is significantly higher in PVNS synovium compared to OA synovium. (**A**) Proportion of all 22 immune infiltration cells based on CIBERSORT in the dataset GSE3698. (**B**) Boxplots visualize the differences of all 22 immune cells calculated by CIBERSORT in OA, RA and PVNS tissues in GSE3698. (**C** and **D**) Immunohistochemistry image for M2 macrophages (CD206; **C**) and Neutrophils (CXCR2; **D**) in the synovium of the patients with OA and PVNS. Scale bar: 50μm (20X) or 20um (40X). *P < 0.05; **P < 0.01.

in OA synovium. To further validate this finding in synovium, we performed immunofluorescence staining on synovium obtained from surgeries of OA, PVNS, and normal tissues (Figure 3E). The staining results indicated that the expression of PDPN shows no significant difference among these three types of synovium, whereas the expression of CD90 varied significantly, with higher levels in PVNS than in OA and normal synovium. This indicated a significant thickening of the sublining structure in PVNS synovium.

https://doi.org/10.2147/JIR.S549953

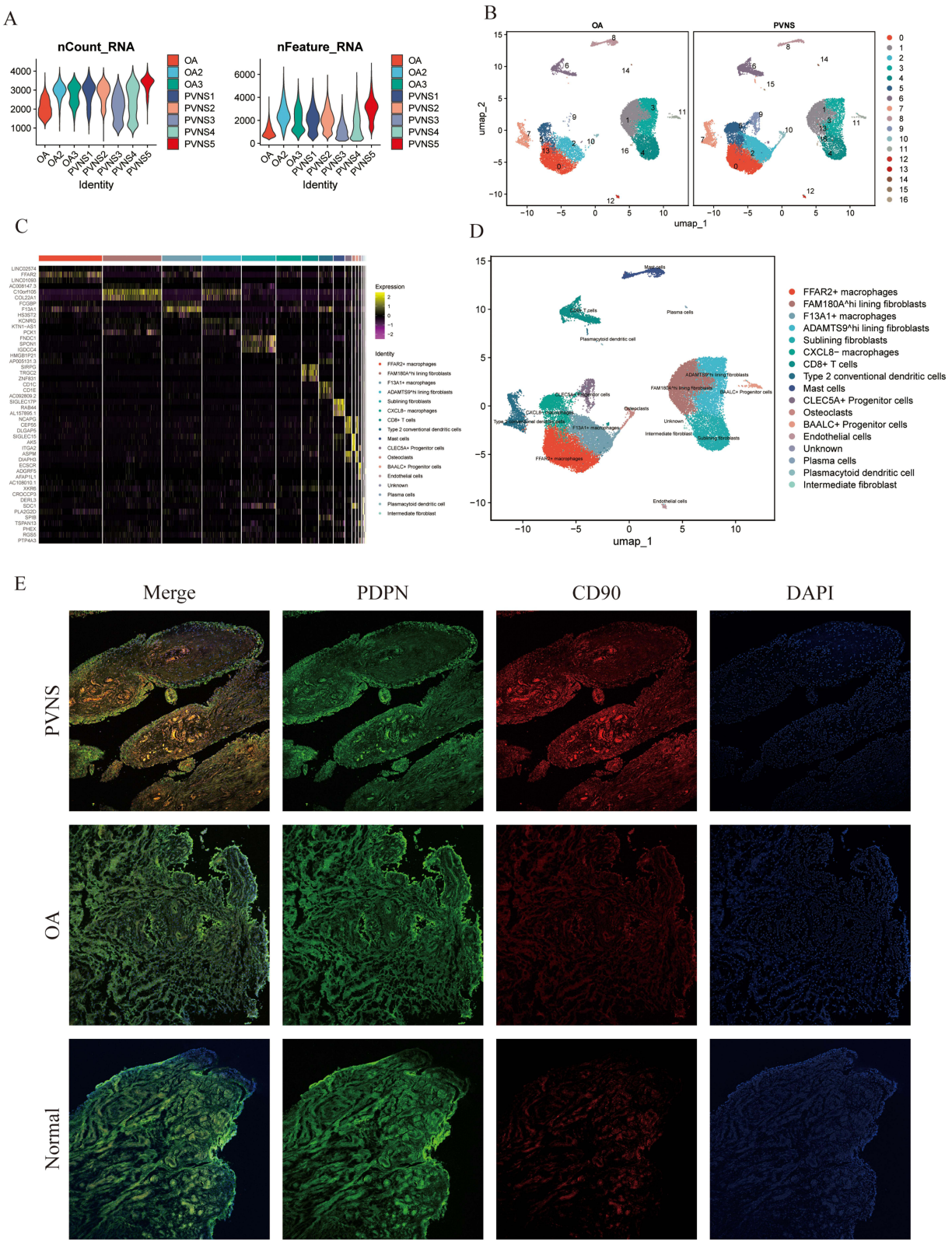

Figure 3 Identification of 16 cell clusters with diverse annotations reveals a high abundance of PDPN(+) CD90(+) sublining fibroblasts in PVNS synovium based on scRNA-seq data. (**A**) Quality control of the scRNA-seq data in GSE155527. (**B**) The UMAP algorithm showing 16 cell clusters after dimensionality reduction. (**C**) Heatmap showing expression of specific gene markers in each cell type. (**D**) The UMAP plot representation demonstrates the main cell types. (**E**) Immunofluorescence images of PDPN and CD90 in the synovium of the normal individuals and patients with OA and PVNS. Red: CD90, Green: PDPN, Blue: nucleus.

The Enhanced Migration and Invasion Capabilities of PDPN+CD90+ FLSs in PVNS Synovium

To further investigate the function of PDPN+CD90+ FLSs in PVNS synovium, we isolated FLSs from PVNS and OA synovium through primary cell culture, combined with flow sorting and immunofluorescence staining analysis. The results indicated that the proportion of PDPN and CD90 double-positive FLSs in PVNS FLSs is 79%, compared to 34.3% in OA (Figure 4A and B).

Subsequently, to study the functional and phenotypic differences of PDPN+CD90+ FLSs in OA and PVNS synovium, we used flow cytometry sorting to extract PDPN+CD90+ FLSs from both PVNS and OA for functional cell assays.

In the transwell invasion and migration assay, we observed that after 12 hours, the number of PVNS FLSs passing through the transwell membrane and matrigel is significantly higher than that of OA FLSs (Figure 4C and D). These results suggested that PVNS FLSs have significantly stronger migration and invasion abilities than OA FLSs. In the wound healing assay, we photographed OA and PVNS FLSs after 12h and 24h migration, respectively. The results suggest that PVNS FLSs have a significantly stronger migration ability than OA FLSs (Figure 4E).

PDPN+CD90+ FLSs in PVNS Synovium Express a Mass of Pro-Inflammatory Cytokines and Invasion Related Proteins

We then compared the PDPN+CD90+ FLSs cells in PVNS and OA tissues using single-cell sequencing data. The results indicate that PDPN+CD90+FLSs cells in PVNS have significantly higher expression of genes related to inducing inflammatory response and bone destruction pathways compared to PDPN+CD90+FLSs cells in OA tissue, including MMP3, MMP9, CCL20, and ACP4 (TNFSF11B) (Figure 5A–D).

We examined the expression of related genes in PDPN+CD90+FLSs cells from OA and PVNS using Western Blot and performed statistical analysis (Figure 5E and F).

The Western Blot results showed that the expression levels of MMP9, M-CSF, IL-1B, and TNF-A in PDPN+CD90 +FLSs cells are significantly higher in the PVNS group than in the OA group. Conversely, the expression level of OPG in the PVNS group was significantly lower than in the OA group (Figure 5E). In summary, PVNS synovium not only showed significant sublining thickening and an increased proportion of PDPN+CD90+FLSs, but also exhibited significantly enhanced abilities to induce inflammatory responses and bone destruction.

Discussion

Pigmented villonodular synovitis (PVNS) is recognized as a borderline tumor with a high recurrence rate and a locally destructive nature.[10] While persistent inflammation is believed to be a key driver of synovial invasion, the underlying mechanisms remain poorly understood and require further elucidation.[11] In this study, we mapped the single-cell sequencing of PVNS tissue using cell classification and gene enrichment analysis to explore the mechanisms of synovial invasion in PVNS. Our findings identify CD90+ FLSs as the primary drivers of synovial invasion, with the potential to induce macrophage polarization. Furthermore, we detailed the molecular mechanisms involved in these processes.

CD90, also known as Thy-1, is a 25–35 kDa glycosylphosphatidylinositol (GPI)-anchored protein belonging to the immunoglobulin superfamily. Human CD90 is expressed in nerve cells, subsets of CD34+ cells, subsets of fetal hepatocytes, subsets of fetal thymocytes, fibroblasts, activated endothelial cells, and certain leukemic cell lines.[12] Thy-1 is involved in cell adhesion, differentiation, and cell-to-cell interactions.[13] It serves as a marker for human microvascular endothelial cell activation and is associated with neovascularization;[14] it is also a crucial marker for the identification of human mesenchymal stem cells (MSCs).[15]

One of the important characteristics of Pigmented Villonodular Synovitis (PVNS) is the significant deposition of pigments, specifically hemosiderin, which is rare in other synovial lesions.[16] For substantial hemosiderin deposition to occur, the synovium in PVNS must have a rich blood supply. Recent studies have shown that CD90 is significantly associated with promoting angiogenesis, forming the tumor microenvironment, and mediating cell-cell and cell-matrix interactions.[17,18] Therefore, CD90 plays an important role in the progression of PVNS. In this experiment, we selected CD90+ FLSs and conducted a series of cellular functional assays. We found that their ability to invade and migrate was

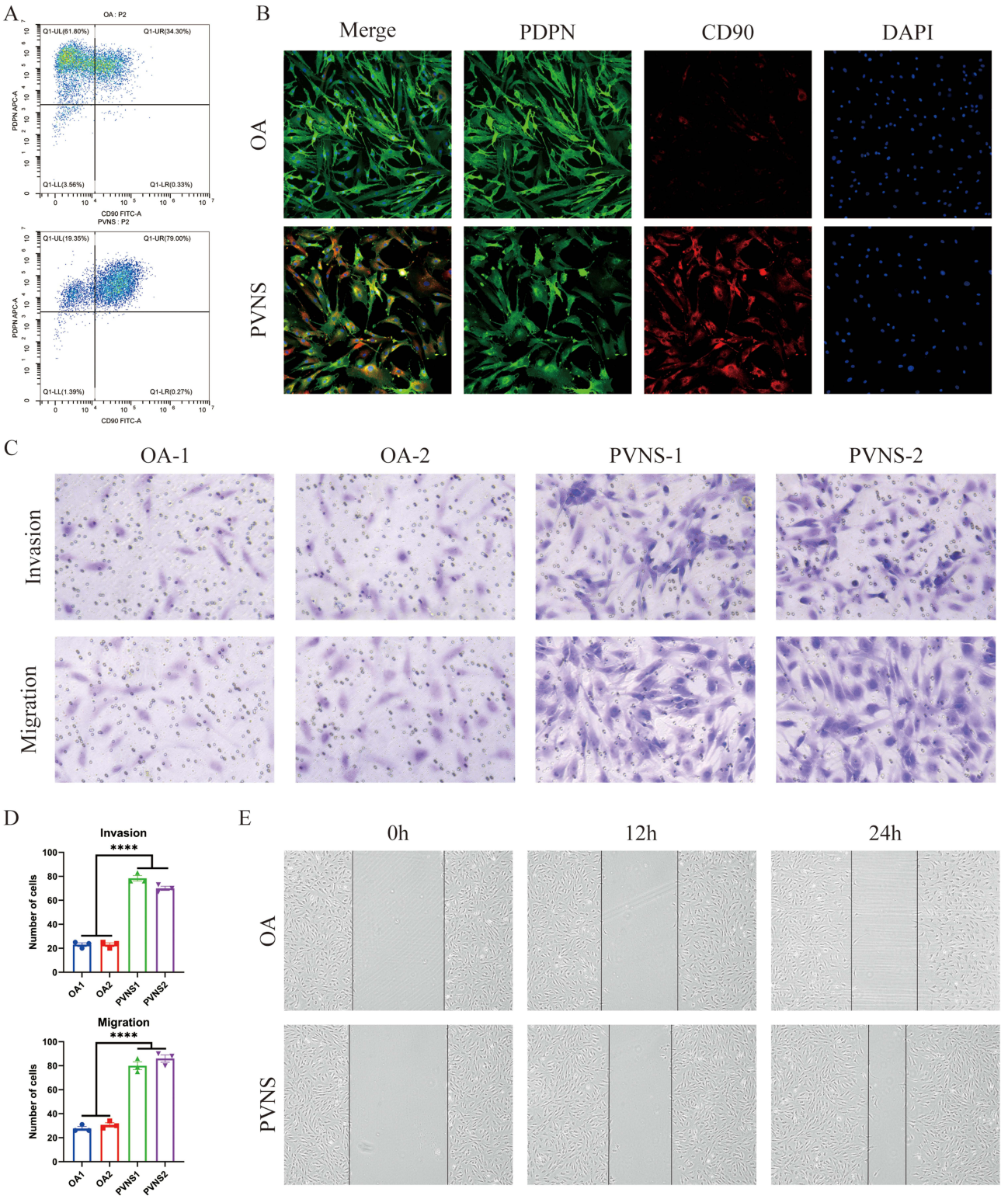

Figure 4 PDPN(+) CD90(+) sublining fibroblasts in PVNS synovium exhibit enhanced migration and invasion capabilities. (**A**) Flow cytometric analysis of PDPN and CD90 double-positive primary FLSs populations in OA (up) and PVNS (down) synovium. (**B**) PDPN and CD90 immunofluorescence image of OA FLSs and PVNS FLSs. Red: CD90, Green: PDPN, Blue: nucleus. (**C**) Transwell migration (lower panel) and invasion (upper panel) assays of OA FLSs and PVNS FLSs. (**D**) Statistical analysis of transwell migration (lower panel) and invasion (upper panel) assays. (**E**) Wound-healing analysis of OA FLSs (up) and PVNS FLSs (down). ****P < 0.0001.

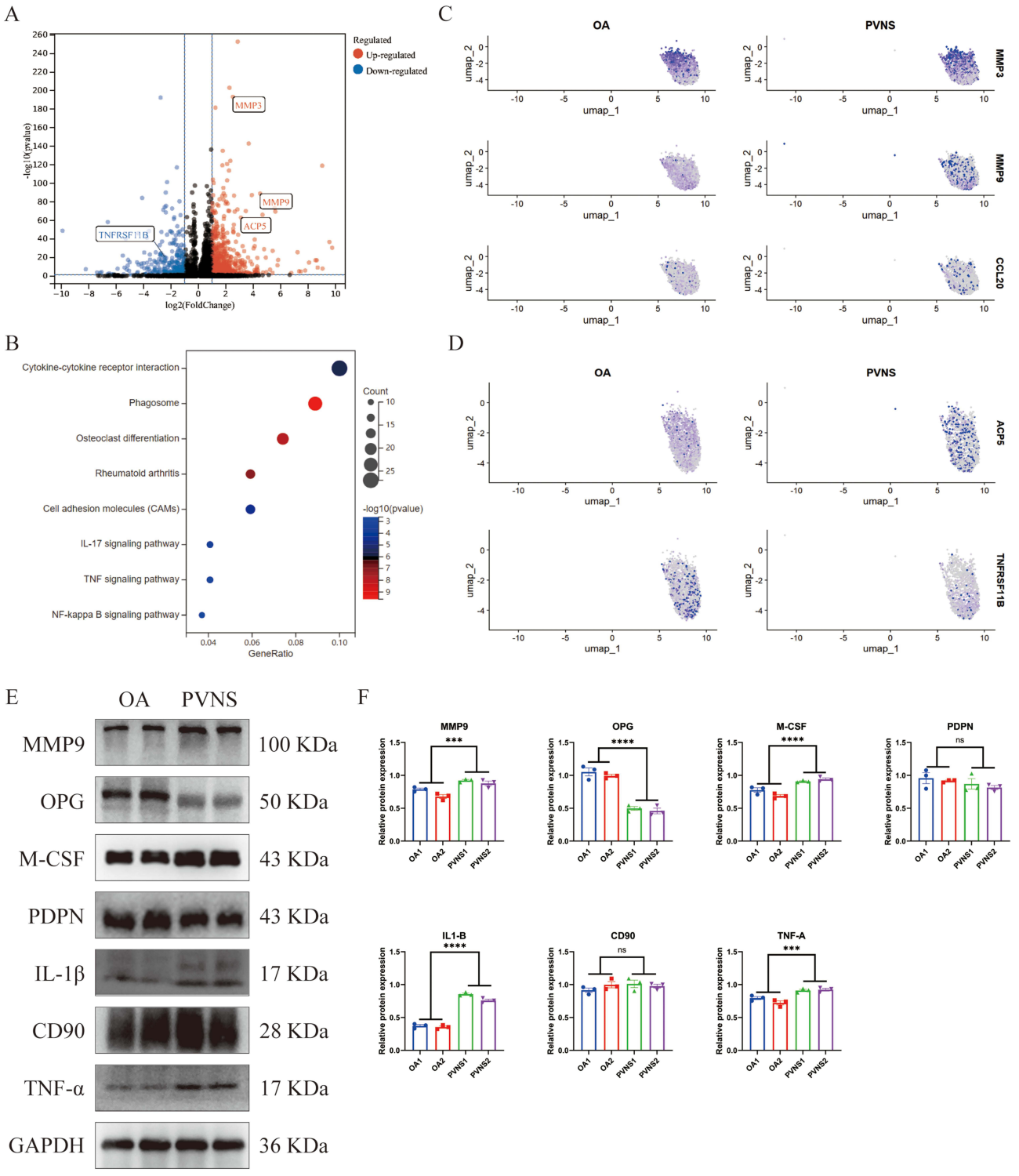

Figure 5 PDPN(+) CD90(+) sublining fibroblasts express higher levels of pro-inflammatory cytokines and invasion related proteins. (**A**) Volcano plot of DEGs in PDPN(+) CD90(+) sublining fibroblasts between the OA and PVNS synovium. (**B**) KEGG pathway analysis of the DEGs. (**C**) UMAP plots showing the expression of inflammatory factors in OA and PVNS PDPN(+) CD90(+) sublining fibroblasts. (**D**) UMAP plots showing the expression of osteoclast-related proteins in OA and PVNS PDPN(+) CD90 (+) sublining fibroblasts. (**E**) Representative images of hub protein expression detected by Western blot. (**F**) Statistical analysis of Western blot. All data are expressed as mean ± SD, n = 3. ns $P > 0.05$; ***$P < 0.001$; ****$P < 0.0001$.

significantly stronger than that of OA FLSs. We also performed Western blot analysis to detect the expression of inflammatory factors, discovering that their expression levels were much higher than those in OA FLSs. Furthermore, through immunofluorescence staining, we localized CD90+ FLSs primarily in the sublayer of PVNS synovium on the

https://doi.org/10.2147/JIR.S549953

tissue level.[11] At the cellular level, it was evident that CD90 expression showed a significant difference between PVNS and OA.

To achieve substantial hemosiderin deposition, a rich blood supply alone is insufficient. Macrophages must engulf the erythrocytes leaked from blood vessels and degrade them through lysosomes to produce hemosiderin. Our immunohistochemistry results indicate the presence of a large number of macrophages in PVNS synovium.[8]

The current research on the mechanisms of PVNS is still significantly lacking.[6] Previous studies have reported that the synovium in OA or RA exhibits characteristics similar to PVNS.[19] However, these studies primarily focused on the lining layer of the synovium, often overlooking the critical role of the sublining layer. Our study demonstrates that the sublining layer of PVNS synovium plays a significant role in recurrence and invasion, distinguishing PVNS from other synovial diseases. These findings could potentially alter the clinical approach to treating PVNS.

Currently, PVNS is considered a subtype of rare, benign proliferative tumors, with a high recurrence rate within one to three months post-surgery.[20] This suggests that in recurrent cases, the surgical removal of the synovium may not have been sufficiently deep to reach the sublining layer. Traditional synovitis treatments, which involve cleaning the inflammatory synovium, may not be effective for PVNS.

These findings provide crucial insights for clinical translation. Targeting CD90+ FLSs could inform more effective surgical strategies that ensure complete removal of the sublining layer, potentially reducing recurrence. Furthermore, our identification of their invasive and inflammatory properties opens avenues for developing targeted therapies against these pathogenic cells. Future research should focus on validating CD90 as a therapeutic target and exploring targeted drug delivery systems to suppress synovial invasion in PVNS.

However, there are limitations in our study that will be the focus of future research. Our experiments did not include in vivo studies, and due to the rarity of PVNS, a recognized experimental animal model for PVNS is still lacking. The absence of a well-established PVNS animal model presents significant challenges for related research. We are currently developing a novel animal model that enables long-term observation of phenotypic changes in PVNS synovial tissue and dynamic monitoring of key gene expression patterns. Although we identified the pathogenic FLSs group in PVNS, further investigation is needed to understand the molecular mechanisms by which these cells contribute to bone and cartilage destruction.

Conclusion

In conclusion, this study provides structural and functional insights into the pathogenic mechanisms of PVNS. We have demonstrated that CD90+PDPN+ FLSs play a pivotal role in driving synovial invasion and promoting bone resorption in PVNS. These findings not only advance our understanding of PVNS pathogenesis but also reveal new therapeutic targets. Future studies should focus on developing targeted strategies to inhibit the invasive and osteoclastogenic functions of these cells, potentially through selective inhibitors, to improve clinical outcomes for PVNS patients.

Abbreviations

PVNS, Pigmented villonodular synovitis; TGCT, Tenosynovial giant cell tumor; OA, Osteoarthritis; RA, Rheumatoid Arthritis; ACL, Anterior cruciate ligament; RNA-seq, RNA sequencing; DEGs, Differentially expressed genes; GSEA, Gene set enrichment analysis; FLSs, Synovial fibroblasts; CD90, Cluster of Differentiation 90; PDPN, Podoplanin; IL-1β, Interleukin-1beta; TNF-α, Tumor Necrosis Factor-α; MMP9, Matrix metalloproteinase-9; OPG, Osteoprotegerin; M-CSF, Macrophage colony-stimulating factor; GAPDH, Glyceraldehyde −3-phosphate dehydrogenase; CSF1, Colony Stimulating Factor 1; CXCR2, C-X-C motif chemokine receptor 2; GEO, Gene Expression Omnibus; KEGG, Kyoto Encyclopedia of Genes and Genomes; PCA, Principal component analysis; DMEM, Dulbecco's modified Eagle's medium; FBS, Fetal bovine serum; IgG, Immunoglobulin G; HRP, Horseradish Peroxidase.

Data Sharing Statement

All data supporting the findings of this study are available within the Article, or are available from the corresponding authors upon reasonable request.

Ethics Approval and Consent to Participate

This study has been performed in accordance with the Declaration of Helsinki and been approved by the ethics committees of Zhu Jiang Hospital of Southern Medical University ethically and provided the corresponding ethical certificate (NO. 2021-KY-165-03) and informed consent. Written informed consent was obtained from each participant after clarification of the study objectives and activities.

Author Contributions

All authors made a significant contribution to the work reported, whether that is in the conception, study design, execution, acquisition of data, analysis and interpretation, or in all these areas; took part in drafting, revising or critically reviewing the article; gave final approval of the version to be published; have agreed on the journal to which the article has been submitted; and agree to be accountable for all aspects of the work.

Funding

This research was supported by Natural Science Foundation of Guangdong Province (Grant no.2022A1515010293), Presidential Foundation of Zhujiang Hospital (Project No. yzjj2023qn25), and National Natural Science Foundation of China (Grant no. 82572792 and 82503822).

Disclosure

The authors declare that they have no competing interests.

References

1. Gounder MM, Thomas DM, Tap WD. Locally aggressive connective tissue tumors. *J Clin Oncol*. 2018;36(2):202–209. doi:10.1200/jco.2017.75.8482
2. Verspoor FG, Zee AA, Hannink G, van der Geest IC, Veth RP, Schreuder HW. Long-term follow-up results of primary and recurrent pigmented villonodular synovitis. *Rheumatology*. 2014;53(11):2063–2070. doi:10.1093/rheumatology/keu230
3. Fiocco U, Sfriso P, Lunardi F, et al. Molecular pathways involved in synovial cell inflammation and tumoral proliferation in diffuse pigmented villonodular synovitis. *Autoimmun Rev*. 2010;9(11):780–784. doi:10.1016/j.autrev.2010.07.001
4. van IDGP, Matusiak M, Charville GW, et al. Interactions in CSF1-driven tenosynovial giant cell tumors. *Clin Cancer Res*. 2022;28(22):4934–4946. doi:10.1158/1078-0432.Ccr-22-1898
5. Spierenburg G, Grimison P, Chevreau C, et al. Long-term follow-up of nilotinib in patients with advanced tenosynovial giant cell tumours: long-term follow-up of nilotinib in TGCT. *Eur J Cancer*. 2022;173:219–228. doi:10.1016/j.ejca.2022.06.028
6. Li T, Xiong Y, Li J, et al. Mapping and analysis of protein and gene profile identification of the important role of transforming growth factor beta in synovial invasion in patients with pigmented villonodular synovitis. *Arthritis Rheumatol*. 2024;76(11):1679–1695. doi:10.1002/art.42946
7. Finis K, Sültmann H, Ruschhaupt M, et al. Analysis of pigmented villonodular synovitis with genome-wide complementary DNA microarray and tissue array technology reveals insight into potential novel therapeutic approaches. *Arthritis Rheum*. 2006;54(3):1009–1019. doi:10.1002/art.21641
8. Zhao Y, Lv J, Zhang H, Xie J, Dai H, Zhang X. Gene expression profiles analyzed using integrating rna sequencing, and microarray reveals increased inflammatory response, proliferation, and osteoclastogenesis in pigmented villonodular synovitis. *Front Immunol*. 2021;12:665442. doi:10.3389/fimmu.2021.665442
9. Heng H, Li D, Su W, et al. Exploration of comorbidity mechanisms and potential therapeutic targets of rheumatoid arthritis and pigmented villonodular synovitis using machine learning and bioinformatics analysis. *Front Genet*. 2022;13:1095058. doi:10.3389/fgene.2022.1095058
10. Cao C, Wu F, Niu X, et al. Cadherin-11 cooperates with inflammatory factors to promote the migration and invasion of fibroblast-like synoviocytes in pigmented villonodular synovitis. *Theranostics*. 2020;10(23):10573–10588. doi:10.7150/thno.48666
11. Damerau A, Rosenow E, Alkhoury D, Buttgereit F, Gaber T. Fibrotic pathways and fibroblast-like synoviocyte phenotypes in osteoarthritis. *Front Immunol*. 2024;15:1385006. doi:10.3389/fimmu.2024.1385006
12. Abebayehu D, Pfaff BN, Bingham GC, et al. A Thy-1-negative immunofibroblast population emerges as a key determinant of fibrotic outcomes to biomaterials. *Sci Adv*. 2024;10(24):eadf2675. doi:10.1126/sciadv.adf2675
13. Valdivia A, Avalos AM, Leyton L. Thy-1 (CD90)-regulated cell adhesion and migration of mesenchymal cells: insights into adhesomes, mechanical forces, and signaling pathways. *Front Cell Dev Biol*. 2023;11:1221306. doi:10.3389/fcell.2023.1221306
14. Foygel K, Wang H, Machtaler S, et al. Detection of pancreatic ductal adenocarcinoma in mice by ultrasound imaging of thymocyte differentiation antigen 1. *Gastroenterology*. 2013;145(4):885–894.e3. doi:10.1053/j.gastro.2013.06.011
15. Muntión S, Sánchez-Luis E, Díez-Campelo M, Blanco JF, Sánchez-Guijo F, De Las Rivas J. Novel gene biomarkers specific to human mesenchymal stem cells isolated from bone marrow. *Int J Mol Sci*. 2024;25(22):11906. doi:10.3390/ijms252211906
16. Robert M, Farese H, Miossec P. Update on tenosynovial giant cell tumor, an inflammatory arthritis with neoplastic features. *Front Immunol*. 2022;13:820046. doi:10.3389/fimmu.2022.820046
17. Zeng F, Gao M, Liao S, Zhou Z, Luo G, Zhou Y. Role and mechanism of CD90(+) fibroblasts in inflammatory diseases and malignant tumors. *Mol Med*. 2023;29(1):20. doi:10.1186/s10020-023-00616-7

18. Wang L, Hu R, Xu P, et al. CD90's role in vascularization and healing of rib fractures: insights from Dll4/notch regulation. *Inflamm Res*. 2024;73 (12):2263–2277. doi:10.1007/s00011-024-01962-w
19. Farese H, Noack M, Miossec P. Synoviocytes from pigmented villonodular synovitis are less sensitive to cadmium-induced cell death than synoviocytes from rheumatoid arthritis. *Sci Rep*. 2022;12(1):3832. doi:10.1038/s41598-022-07745-9
20. Song HQ, Wu GF, Qi WZ, Lin LJ. Diffuse pigmented villonodular synovitis treated with arthroscopic total synovial peel. *BMC Surg*. 2023;23 (1):12. doi:10.1186/s12893-023-01906-x